

# Excellence in Chemistry Research

## Announcing our new flagship journal

- Gold Open Access
- Publishing charges waived
- Preprints welcome
- Edited by active scientists



## Meet the Editors of *ChemistryEurope*



**Luisa De Cola**

Università degli Studi  
di Milano Statale, Italy



**Ive Hermans**

University of  
Wisconsin-Madison, USA



**Ken Tanaka**

Tokyo Institute of  
Technology, Japan

# Spray-coated Hard Carbon Composite Anodes for Sodium-Ion Insertion

Krishnaveni Palanisamy,<sup>[a]</sup> Sven Daboss,<sup>[a]</sup> David Schäfer,<sup>[b]</sup> Marcus Rohnke,<sup>[b]</sup> Laurin Derr,<sup>[c]</sup> Marcel Lang,<sup>[c]</sup> Rolf Schuster,<sup>[c]</sup> and Christine Kranz<sup>\*[a]</sup>

Sodium-ion batteries are among the most promising alternatives to lithium-ion batteries. Hard carbon (HC) electrodes have been recognized as suitable active anode material for mono-valent ion batteries. Here, we present a simple and cost-effective spray-coating process to prepare HC composite electrodes on copper current collectors with different binder (sodium carboxymethyl cellulose, CMC) content and different HC particle sizes. The spray-coated electrodes were evaluated and tested in 1 M sodium perchlorate (NaClO<sub>4</sub>) in propylene carbonate (PC) in dependence of the CMC content with and without fluoroethylene carbonate (FEC) as additive, and the performance was also compared to doctor bladed HC electro-

des. Spray-coated anodes in Na half-cells revealed improved capacity during the first cycles compared with doctor bladed anodes with similar thicknesses. Time-of-flight secondary ion mass spectrometry (ToF-SIMS) studies were performed, which revealed a significant increase of inorganic fluoro-compounds in the formed solid electrolyte interphase (SEI) when FEC was present as additive. In addition, first single electrode microcalorimetry studies on spray-coated thin HC composite electrodes yielded an entropy of the sodiation process of 80 J mol<sup>-1</sup> K<sup>-1</sup> at high state of charge (SoC), comparable to that of bulk Na deposition.

## Introduction

Developing energy storage systems to meet the requirements for the fast growing markets of small, lightweight, thin, and flexible electronic devices<sup>[1]</sup> drives research of post-lithium mono-valent battery chemistries like sodium (Na)-ion batteries (SIBs)<sup>[2]</sup> and to a smaller extent potassium (K)-ion batteries (PIBs)<sup>[3]</sup> given the earth abundance of these elements. Hard carbon (HC) has been recognized as a highly suitable anode material for alkali-ion batteries, particularly for Na.<sup>[4,5]</sup> Despite recent studies focusing on the preparation of HC anode materials and the investigation of insertion mechanisms, the sodiation/desodiation process in HC and the formation of interphases is still not fully understood. A challenge is the higher solubility of solid electrolyte interphase (SEI) compounds

in SIBs dependent on parameters like electrolyte composition and temperature compared to LIBs.<sup>[6]</sup> Also, the different synthesis routes for HC, which result in quite varying performances<sup>[7]</sup> hamper a comprehensive evaluation. Reproducible fabrication of HC electrodes is required ensuring controlled mass loading to make performance data comparable. Considerable efforts have been dedicated towards the preparation process of composite electrode materials mainly for Li-ion batteries (LIBs) such as doctor blade (DB) coating,<sup>[6,7]</sup> or printing processes like spray-printing,<sup>[10]</sup> dry-printing technology,<sup>[11]</sup> electrophoretic deposition,<sup>[12]</sup> electrostatic spray deposition,<sup>[13]</sup> spray deposition,<sup>[14]</sup> slot die coating,<sup>[15]</sup> ink-jet printing,<sup>[16]</sup> and comma bar coating<sup>[17]</sup> to obtain uniformly thin films with controlled mass of the active material for cycling tests. A remaining challenge in coatings is related to the delamination of the active material during cycling in SIBs. The stability on the current collector depends, among other factors, on the preparation technique and the distribution of the binder during the drying process.<sup>[18]</sup> Spray-coating has emerged as a pivotal technique in surface modification offering advantages like uniform coatings, uniform distribution of the components and deposition of thin layers of active materials with controlled layer thickness. Spray-coating techniques have been employed to produce electrodes for solar panel superhydrophobic thin-film coatings,<sup>[19]</sup> cathodes for LIBs,<sup>[14]</sup> and activated carbon /single-/few-layer graphene (SLG/FGL) composites for electrochemical double-layer capacitors (EDLCs).<sup>[20]</sup> For wearable LIBs electrodes, binder-assisted electrostatic spray deposition has been reported to coat interdigitated current collectors on flexible polyimide films.<sup>[13]</sup> For SIBs anode fabrication, mainly DB coating is used.<sup>[9]</sup> However, issues with DB, like the polarity of graphitic surfaces may lead to precipitations or aggregations of HC particles and finally to instable low-quality films. In addition,

[a] K. Palanisamy, Dr. S. Daboss, Prof. Dr. C. Kranz  
Institute of Analytical and Bioanalytical Chemistry  
Ulm University  
Albert-Einstein-Allee 11, 89081 Ulm (Germany)  
E-mail: christine.kranz@uni-ulm.de

[b] D. Schäfer, Dr. M. Rohnke  
Institute of Physical Chemistry, Center for Materials Research  
Justus Liebig University of Giessen  
Heinrich-Buff-Ring 17, 35392 Giessen (Germany)

[c] L. Derr, Dr. M. Lang, Prof. Dr. R. Schuster  
Institute of Physical Chemistry  
Karlsruhe Institute of Technology  
Fritz-Haber-Weg 2, 76131 Karlsruhe (Germany)

Supporting information for this article is available on the WWW under <https://doi.org/10.1002/batt.202300402>

© 2023 The Authors. Batteries & Supercaps published by Wiley-VCH GmbH. This is an open access article under the terms of the Creative Commons Attribution License, which permits use, distribution and reproduction in any medium, provided the original work is properly cited.

the DB coating process typically involves the blade spreading of the active material onto the substrate, which limits the size and scalability of the process for thin coatings, while in contrast, spray-coating<sup>[20]</sup> can be easily integrated into existing manufacturing processes, enabling seamless production at large scale. In addition, spray-coating facilitates the use of masks. Specific geometries of composite electrodes with defined thickness can be obtained, which is more challenging using DB.

Due to their high electrochemical stability, carbonate-based electrolytes, mainly propylene carbonate (PC) in combination with sodium perchlorate (NaClO<sub>4</sub>) – primarily employed for laboratory studies or sodium hexafluorophosphate (NaPF<sub>6</sub>) are used in half-cells of SIBs.<sup>[21,22]</sup> Although SIBs are at the verge of commercialization, there are still challenges associated with degradation of both, anode and cathode active material, along with chemical reactions occurring during sodiation/desodiation and SEI dissolution.<sup>[5,23,24]</sup>

The electrochemical storage mechanism<sup>[25]</sup> relies on the insertion of Na<sup>+</sup> ions, chemical reactions with the electrolyte,<sup>[24,26]</sup> or decomposition of the electrolyte,<sup>[21,27]</sup> which limits both cycling stability and specific capacity. For instance, the insertion of Na<sup>+</sup> ions into HC particles causes changes in the structure of sodiated HC.<sup>[25]</sup> The arrangement of HC particles along with other components of the composite like binders such as polyvinylidene fluoride (PVDF),<sup>[28]</sup> and water soluble carboxymethyl cellulose (CMC),<sup>[29,30]</sup> conductive carbon (CC) and the resulting electrode structure can be the reason for capacity fading, significantly affecting the insertion of charge carriers.<sup>[31]</sup> Binder contents are typically in the range of 5–10% and it is known that the binder content plays a significant role in the battery performance.<sup>[32,33]</sup> It has been reported that HC anodes cycled in NaPF<sub>6</sub>/PC showed improved averaged coulombic efficiency and better capacity retention when CMC was used as binder in comparison to PVDF.<sup>[30]</sup> In general, water soluble binders like CMC are reported to support the more uniform distribution of the active material.<sup>[28]</sup> In addition, the rate capability of SIBs is affected by thickness of both anode and cathode, while high energy density can be achieved at low current rates.<sup>[34,35]</sup> To overcome such limitations, several strategies are pursued: controlling the electrode coating thickness on the current collector, managing the mass loading of the active material, achieving balanced porosity in the electrodes to optimize the interaction with the electrolyte, and selecting appropriate solvent/solvation molecules to extend the cycling stability.<sup>[36,37]</sup> Wang et al. discussed optimization strategies for the preparation process of HC composite anode materials and presented the performance in different electrolytes for RT SIBs.<sup>[38]</sup> The same group also reviewed studies of reaction mechanisms of HC anode materials by in situ TEM experiments.<sup>[39]</sup> Overall, for HC composite anodes high volumetric energy, appropriate thickness, and long-term cycle stability are required.<sup>[40–42]</sup> Spray-coating is a possible route for accurately adjusting the thickness of the electrode, which becomes particularly important for the fabrication of thin HC layers. Such thin coatings with controlled mass loading are a prerequisite for studies like electrochemical microcalorimetry, as demonstrated in this contribution. Good thermal conductance is

required that can be achieved by thin coatings to ensure fast heat transfer and thermal equilibration.<sup>[43,44]</sup> Compared with the main technique used for coating such as DB, spray-coating as a non-contact method applies less mechanical stress to the current collector and the active electrode materials, which may be advantageous e.g., for polymeric active materials. As a pre-metered-coating technique, the applied coating weight is not dependent on the process. Here, the number of passes is the main determining factor for the coating thickness and mass loading. Spray-coating can be used with a wide range of electrode materials and formulations, making it versatile for different battery chemistries.

The performance of SIBs is strongly dependent on SEI formation. However, SEI formation on HC is not yet fully characterized, and it is strongly dependent on various parameters like solvent and used salt as well as additives and the fact whether half- or full-cell experiments are performed.<sup>[45]</sup> Among available additives, fluoroethylene carbonate (FEC) proved to be an effective additive to promote SEI formation on HC in half-cells.<sup>[21,46]</sup>

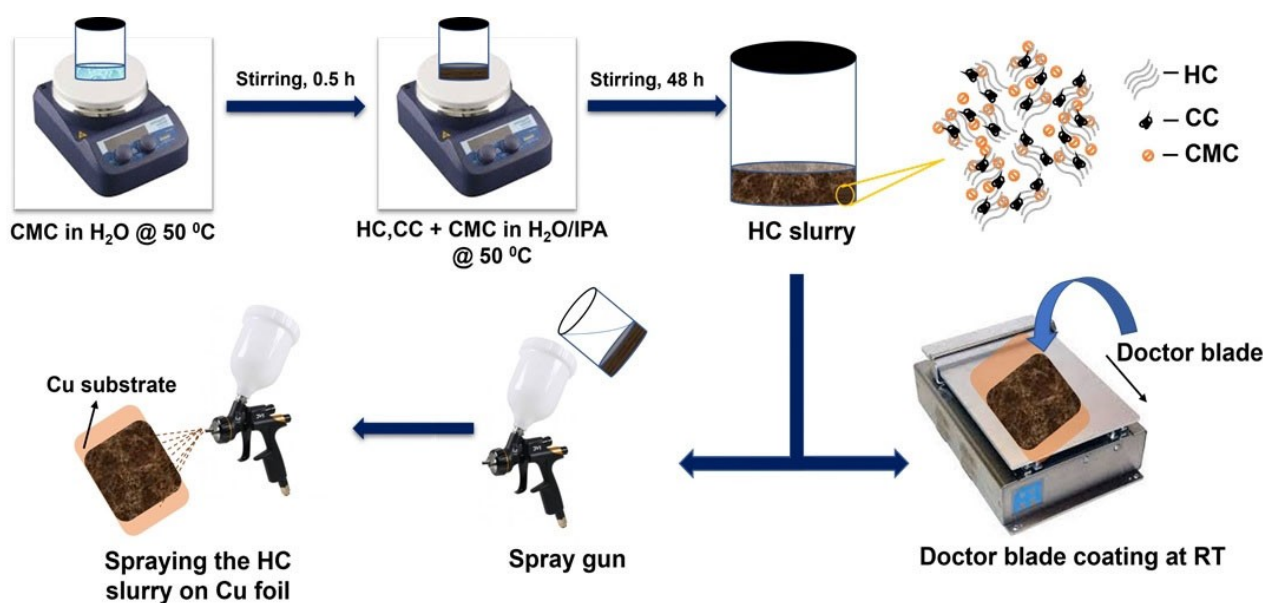
In the literature, the formation and the properties of the SEI are mainly studied by transmission electron microscopy (TEM),<sup>[47]</sup> cryo-TEM,<sup>[48,49]</sup> or X-ray photoelectron spectroscopy (XPS)<sup>[26,47]</sup> as recently reported. A recent study focused on the heterogeneity of the formed SEI on HC composite anodes used in half-cell experiments after cycling in 1 M NaClO<sub>4</sub> in PC along with FEC as additive by conductive atomic force microscopy (AFM) and AFM-scanning electrochemical microscopy (SECM).<sup>[50]</sup> In addition, nanomechanical properties were correlated to the composition of the electrolyte and presence of SEI. However, the chemical composition of the SEI could not be accessed with these techniques.

In the present study, we introduce a simple spray-coating process for the preparation of HC composite anodes (5 μm, type II, 9 μm type I and II) with controlled mass loadings and tunable thickness, which can be achieved by varying the number of passes. The motivation of the lab scale coating process is to produce HC composite electrodes, which can be reproducibly fabricated to study the influence of binder content, SEI formation and composition as well as first thermodynamics insights of sodiation/desodiation process using single electrode microcalorimetry that requires thin films. In addition, these electrodes are systematically studied to correlate the performance with mass loading, thickness, electrode porosity, cycling performance and coulombic efficiency (CE). We present time-of-flight secondary ion mass spectrometry (ToF-SIMS) to study the influence of additive (FEC) on the composition of the formed SEI. First thermodynamic insights into the entropy of Na<sup>+</sup> ion insertion into HC particles is obtained from microcalorimetric measurements of cycled HC electrodes. Characterization studies like ToF-SIMS and microcalorimetry presented here have been obtained with composite HC electrodes containing HC particles (5 μm, type II Kuranode) and 5% of binder obtained with 3 deposition passes.

## Results and Discussion

### Electrode preparation by spray-coating

Scheme 1 illustrates the preparation process for spray-coated HC composite anodes. HC composite electrodes were prepared with different hard carbon particle sizes (Kuranode 5  $\mu\text{m}$  (type II) and 9  $\mu\text{m}$  (type I and II)) and different percentages of CMC ranging from 2.5% to 10% to investigate the performance parameters of the composite electrodes in dependence of the binder content (details of the preparation process are shown in the experimental part). The advantage is that masks can be used during spray-coating, which allows to design the geometric form and area as shown for composite electrodes for microcalorimetry (Figure S1).



Scheme 1. Preparation scheme of spray-coated HC electrodes.

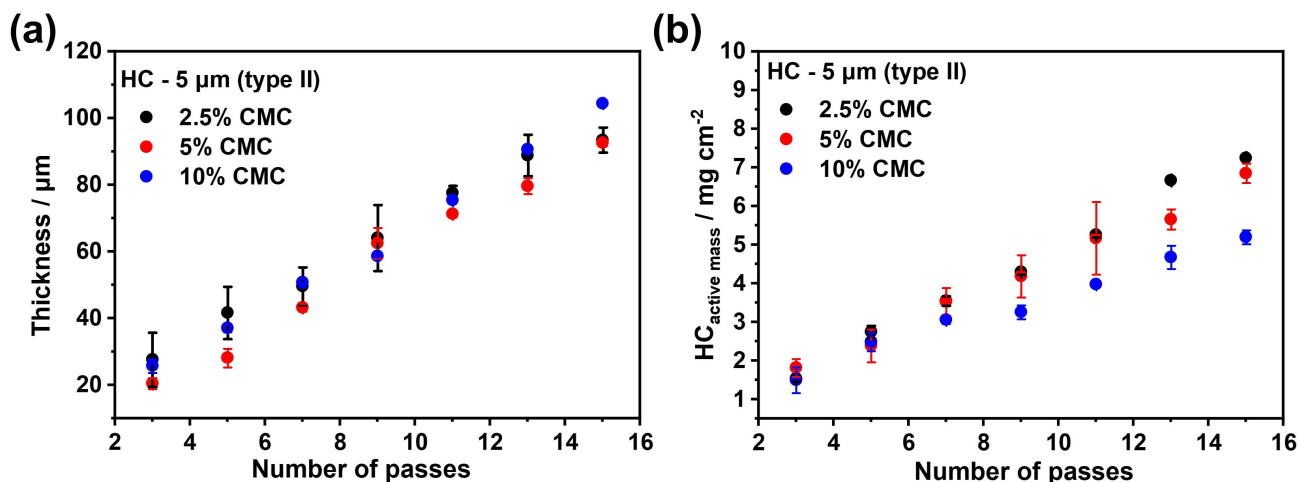


Figure 1. Thickness and mass loading of spray-coated HC - 5  $\mu\text{m}$  (type II) composite electrodes. (a) Thickness of spray-coated HC composite electrodes. (b) Active mass loading per  $\text{cm}^2$  with 2.5%, 5% and 10% binder. Number of passes: 3 to 15 passes. Error bars reflect three different samples with three measurement spots per sample ( $n=3$ ).

$r=6$  mm). The weight of the active mass of HC varied from  $1.82 \pm 0.23$  mg to  $6.85 \pm 0.25$  mg for 3 to 15 passes, respectively. A similar trend was observed for  $9 \mu\text{m}$  (type I) and  $9 \mu\text{m}$  (type II) HC particle sizes with three different binder concentrations as shown in Figure S2. For higher number of passes, we noticed that the binder content has an influence on the mass loading, as the linear relationship deviated slightly for 10% binder applying more than approx. 10 passes. This was not yet systematically studied for HC composite electrodes, however for LIBs recently the role of binder content with respect to the dispersibility was studied for graphite composite anodes.<sup>[51]</sup>

The average surface roughness ( $S_a$ ) of all spray-coated HC electrodes was analyzed by 3D laser scanning microscopy, as shown in Figure S3. No obvious trend of surface roughness was observed independently of particle size and binder content. For example, composite electrodes ( $5 \mu\text{m}$ , type II) containing 2.5% binder show a  $S_a$  value of  $2.41 \pm 0.28 \mu\text{m}$  (measurements were obtained from three spray-coated electrodes at 4 different spots; probed area  $200 \times 200 \mu\text{m}^2$ ). Increasing the content of binder resulted in a slight increase of the surface roughness of the spray-coated HC composite electrodes, which may be explained by the orientation of the HC particles that are more confined and dispersed in higher binder content. The observed trend towards higher  $S_a$  values of the HC composite electrodes with  $9 \mu\text{m}$  particles at higher binder content (5% and 10%) may also be related to an increased viscosity of the slurry and with that also to prolonged drying times.

Overall, optimization of the mass loading of active material on either the anode or cathode side has a crucial impact, as the thickness of the coating is among the reasons of the failure of batteries, as thick coatings suffer from fracture and delamination after coating and drying.<sup>[52]</sup> Any mass loading ratio between anode and cathode materials can easily be accessed with the spray-coating technique by the number of passes.

### Morphological and structural characterization of the spray-coated HC composite electrodes

The microstructure and morphological features of spray-coated HC ( $5 \mu\text{m}$  (type II)) electrodes with different binder content were analyzed via SEM as shown in Figure S4(a–c). Notably, a stable and crack-free film was obtained when dispersing the slurry via spray-coating. The cross-sections of the corresponding top view images presented in Figure S4(d–f) show similar appearance of the composite electrode and distribution of active material and CC. The thickness of the coatings with 2.5%, 5% and 10% binder were determined by 3D laser scanning microscopy on the Cu substrate with film thicknesses of  $27.7 \pm 8.1$ ,  $20.5 \pm 0.7$  and  $25.8 \pm 2.0 \mu\text{m}$  ( $n=3$ ), respectively. We also fabricated HC composite electrodes by DB coating with similar thicknesses ( $20.2 \pm 0.3 \mu\text{m}$ ,  $n=3$ ) to compare the electrochemical performance of the spray-coated HC electrodes and doctor blade electrodes. The microstructure of the DB-coated electrodes showed similar arrangement of HC particles within the composite compared to the spray-coated electrodes. The observed weight of the active mass loading of the HC ( $9 \mu\text{m}$

composite electrodes with 5% binder was  $4.0 \pm 0.3$  (type I) and  $4.1 \pm 0.4$  mg (type II), respectively. The observed thickness for the DB-coated HC composite electrode was  $35.9 \pm 1.0$  (type I) and  $37.7 \pm 1.0 \mu\text{m}$  (type II), respectively. Three replicate samples were investigated.

The microstructural properties of spray-coated HC electrodes, in particular its microporosity with different binder compositions and degree of graphitization are known to have a strong influence on the electrochemical performance.<sup>[5]</sup> We recorded Raman spectra of the HC particles (Raman laser spot size of  $0.5 \mu\text{m}$ ) of the spray-coated HC composite electrodes of all investigated particle sizes which are shown in Figure S5(a–c) for  $5 \mu\text{m}$  (type II),  $9 \mu\text{m}$  (type I and type II) HC composite electrodes, respectively. The Raman spectrum of HC exhibits two characteristic bands: the D band at  $1312 \text{ cm}^{-1}$  and the G band at  $1590 \text{ cm}^{-1}$  corresponding to the defect-induced mode and the  $E_{2g}$  graphitic mode, respectively.<sup>[53]</sup> The intensity ratio of the D band to G band ( $I_D/I_G$ ) ratio is used as indication of the graphitization degree of the samples with different particle sizes of HC. The increase in  $I_D/I_G$  ratio suggests a higher degree of defects/disordered structure of HC particles for both 5 and  $9 \mu\text{m}$  (type II) particles.<sup>[54,55]</sup> In addition, Raman spectra were collected of the as obtained HC and CC powders. The  $I_D/I_G$  ratio for CC is significantly smaller compared to HC type II particles (Figure S5d), due to larger number of defects and disordered structure of the HC particles.

XRD measurements were also conducted to analyze the structural changes induced by  $\text{Na}^+$  ion insertion into HC, as previously shown<sup>[56]</sup> and as depicted in Figure S6(a). The Bragg peak centered at  $2\theta$  ( $\text{Ag } K_\alpha$ ) =  $8.04^\circ$  is assigned to the parallel stacking of graphene sheets of pristine HC. At an applied potential of 0.2 V vs.  $\text{Na}^+/\text{Na}$ , the reflex slightly shifted to a lower angle of  $2\theta = 7.72^\circ$ , indicating an increase in the interlayer distance between the graphene sheets as a result of  $\text{Na}^+$  ion intercalation, as previously reported for sodiation of HC.<sup>[46]</sup> It is assumed that a larger interlayer spacing ( $d = 3.96 \text{ \AA}$ ) and smaller crystallite size of parallel graphene layers in HC compared to graphite ( $d = 3.354 \text{ \AA}$ ) are responsible for  $\text{Na}^+$  ion intercalation between graphene layers.<sup>[46,57]</sup> The variation of the average interlayer distance of  $\text{Na}^+$  ion insertion in between the graphene sheets was estimated from XRD patterns, which is displayed in Figure S6b. The results show that the distance steadily increases as a function of the stored charge which is shown in Figure S6c. With respect to the potential scale, the strongest changes of  $d$  occur in the plateau region near 0.01 V vs.  $\text{Na}^+/\text{Na}$  according to the specific capacity values between 180 and  $360 \text{ mAhg}^{-1}$  (see Figure S6c), implying that another insertion mechanism might be operative in the lower potential range.<sup>[58,59]</sup> Overall, these results reveal that spray-coated HC composite electrodes show similar performance for  $\text{Na}^+$  ions insertion in 1 M  $\text{NaClO}_4$  in PC as reported in the literature.<sup>[46]</sup>

### Electrochemical performance of the spray-coated HC electrodes

Although, Na half-cell experiments are controversially discussed in the literature depending on the used solvent, as they may not be predictive for rate capabilities in full-cells,<sup>[60]</sup> we performed our initial experiments in Na half-cells using NaClO<sub>4</sub> in PC as electrolyte, which have also been used for *operando* characterization studies of the HC sodiation/desodiation mechanism.<sup>[61]</sup> Besides discussions regarding reactions and the impact of metallic Na in carbonate electrolytes,<sup>[22]</sup> also minimal to no reaction of Na in PC, in the presence of 1 M NaClO<sub>4</sub> was reported.<sup>[62]</sup> Figure 2 represents cyclic voltammograms (CVs) recorded of the spray-coated HC composite electrodes with 5% binder, upon sodiation and desodiation in 1 M NaClO<sub>4</sub> in PC with and without FEC as additive. Similar profiles in the first cycle and following cycles are visible for the CVs recorded in presence and absence of the additive. The first cathodic scans (black curves) show two main processes. The plateau observed between 1.25 V and 0.25 V vs. Na<sup>+</sup>/Na is generally attributed to the storage of Na<sup>+</sup> ions at defect sites and surface terminal groups of the HC.<sup>[63]</sup> Electrolyte decomposition and SEI formation typically also fall within this range and might show up as small peaks in the first scans (see insets in Figures 2 and S7). At a potential lower than 0.25 V vs. Na<sup>+</sup>/Na, Na<sup>+</sup> ion insertion into the carbon structure of both CC and HC occurs,<sup>[64,65]</sup> before close to 0 V Na deposition into pores begins.<sup>[59]</sup> The insets in Figure 2 and Figure S7 show the onset potential of the aforementioned main process of storage of Na<sup>+</sup> ions, electrolyte decomposition and Na<sup>+</sup> insertion for HC composite electrodes in the first cathodic scan.

The same experiments were performed with composite electrodes containing 2.5%, 10% binder, as well as a calendared spray-coated electrode containing 5% binder and for comparison a DB-coated HC composite electrode with the same binder content. The results are summarized in Figure S7. The CVs recorded at the electrode containing 5% binder (Figure 2a) exhibit similar current densities in the electrolyte decomposi-

tion potential region when compared to the composite electrodes with 2.5% and 10% binder content. After the first cathodic scan of the HC composite electrodes with 2.5% binder, lower current densities were observed at potentials lower than 0.25 V, when compared to 5% binder content, which further dropped in the following scans (only first three cycles are displayed in Figure S7a). This may be an indication that the low binder content (2.5%) leads to a higher amount of irreversible sodium trapping, which may be also related to thicker or inhomogeneous SEI formation.<sup>[66]</sup> Moreover, electrodes containing 2.5% binder exhibit also a slightly broader de-insertion peak in the low potential region (0.1 V vs. Na<sup>+</sup>/Na) indicating a slower kinetic of the sodiation/desodiation reaction (Figure S7a) when compared to the 5% CMC-based HC electrodes. In contrast, for 10% binder content, the scans were similar in current density to the ones observed for 5% binder, however, stronger capacity fading was observed for 10% binder (Figure 3b), which will be discussed in the next paragraph. The current density of the desodiation process of the HC electrode with 5% CMC remains comparatively constant in the first 3 cycles in comparison to HC composite electrodes with 2.5% and 10% binder, where the current density drop is more prominent.

The impact of the negatively charged binder may be a reason for the observed differences in the CVs of the composite electrodes with different binder content, similar to findings for Zn-ion batteries, where it was proposed that the negatively charged binder may accelerate the intercalation by electrostatic attraction.<sup>[67]</sup> In addition at higher binder contents, the active particle surface becomes partially unavailable for electrochemical reaction, which negatively impacts the performance due to the reduced active area, as shown in the literature for carbon-binder networks for LIBs.<sup>[68]</sup> For low binder contents, an increase of the ion transport resistance might negatively impact the electrode performance.

We also investigated the effect of calendaring on the spray-coated electrodes with 5% binder. Tapped density and electrode porosity are essential parameters for high volumetric capacity and good initial coulombic efficiency. Bedda et al. have

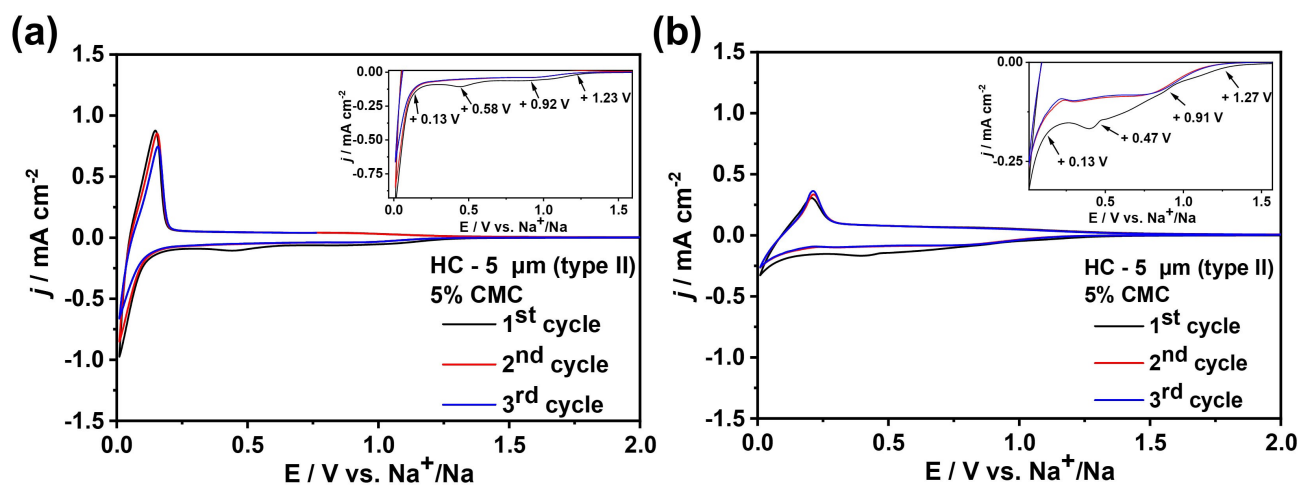
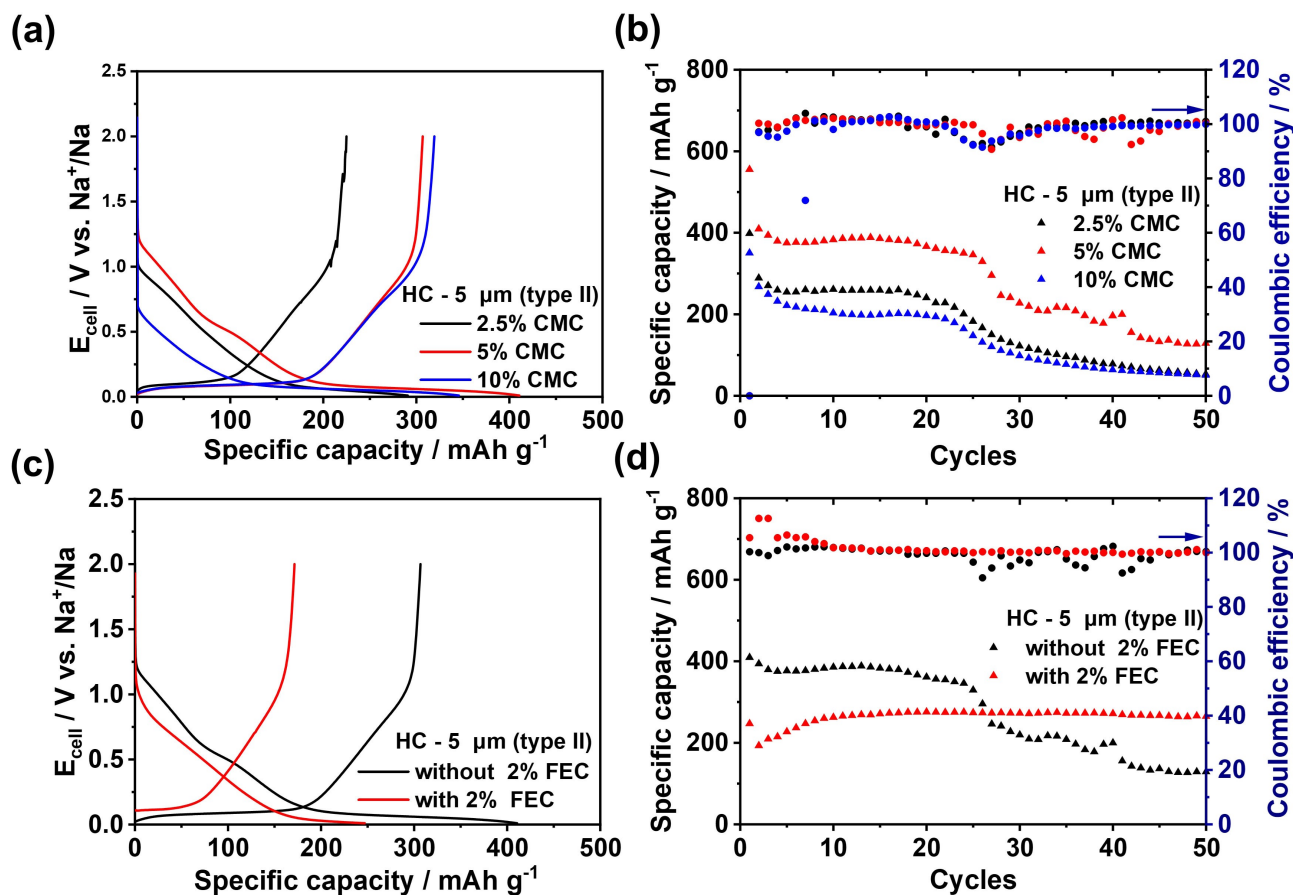


Figure 2. CVs of spray-coated HC electrodes with 5% binder (5 μm (type II)). (a) In 1 M NaClO<sub>4</sub> in PC, (b) 1 M NaClO<sub>4</sub> in PC/2% FEC. Scan rate: 0.1 mV s<sup>-1</sup>, potential range 0.01–2.00 V vs. Na<sup>+</sup>/Na.



**Figure 3.** (a) First discharge-charge voltage profiles (current density =  $20 \text{ mA g}^{-1}$ ) of HC composite electrodes with 2.5% (solid black), 5% (solid red) and 10% (solid blue) binder. (b) Specific capacity (triangles 2.5% black, 5% red and 10% blue) and CE (circles 2.5% black, 5% red and 10% blue) of  $5 \mu\text{m}$  (type II) HC electrodes. (c) First discharge-charge voltage profiles of HC composite electrodes (5% binder,  $5 \mu\text{m}$  (type II) with and without 2% FEC additive). (d) Specific capacity and CE of HC composite electrodes (5% binder,  $5 \mu\text{m}$  (type II) with and without 2% FEC additive. Electrolyte: 1 M  $\text{NaClO}_4$  in PC, current rate of 0.1 C, potential range 0.01–2.00 V vs.  $\text{Na}^+/\text{Na}$ . Triangles (red and black) reflect the specific capacity, and CE values are displayed as circles.

shown that calendaring resulted in improved performance of HC composite anodes with hard carbon spheres of controlled size and shape.<sup>[54]</sup> Hence, we also prepared calendared spray-coated HC composite electrodes, which revealed a similar morphology compared to the non-calendared electrodes.

A decrease in current densities was observed and less reversibility of the sodiation/desodiation process was noted compared to the uncalendared sample (Figure S7c). We assume, this is related to a change in the composite electrode porosity and possibly the re-arrangement of HC particles within the composite due to the calendaring. Besides, the sodiation process occurring below 0.25 V vs.  $\text{Na}^+/\text{Na}$  shows sluggish kinetics similar to the composite electrode with 2.5% binder, as indicated by broad peaks (Figure S7c).

Figure S7d shows the CVs of the DB-coated HC composite electrode with 5% binder. Like the calendared spray-coated sample (Figure S7c), the current densities are decreased for the sodiation/desodiation process. Reduced current densities were observed in the plateau region between 1.25 V to 0.25 V vs.  $\text{Na}^+/\text{Na}$  compared to the three different percentages of binder content of the spray-coated electrodes. Hence, spray-coating seems to be attractive for thin film coatings of HC composite

electrodes compared to the DB coating due to increased insertion of  $\text{Na}^+$  ions.

CVs were also recorded in presence of FEC for the composite electrode with 5% binder as shown in Figure 2(b). Although decreased current densities at potential lower than 0.25 V vs.  $\text{Na}^+/\text{Na}$  were observed, the plateau region between 1.25 V to 0.25 V vs.  $\text{Na}^+/\text{Na}$  in presence of FEC showed increase in current density, most pronounced in the first scan, indicating an increased electrolyte decomposition. Besides, the sodiation process occurring below 0.25 V presents sluggish kinetics compared to the HC composite electrode in absence of FEC as indicated by the broad peak.

The electrochemical behavior upon sodiation was further investigated by galvanostatic cycling tests in 1 M  $\text{NaClO}_4$  in PC also with and without FEC. Figure 3 illustrates the galvanostatic cycling behavior of the initial cycles of the HC composite electrodes with three different percentages of binder upon charge and discharge of  $\text{Na}^+$  ions, respectively. Figure 3(a) shows the cycling behavior of the HC composite electrodes in dependence of the CMC binder content (2.5%, 5% and 10%) at a current rate of  $20 \text{ mA g}^{-1}$  in Na half-cells, which are similar independent of the binder content. In the first discharge cycle,

the specific capacity of HC composite containing 5% binder is slightly lower when compared to the electrode with 10% binder (Figure 3a). However, the following cycles show higher capacity for 5% binder when compared to 10% binder (Figure 3b). In Figure 3b, the coulombic efficiency and the specific capacity are displayed. All three HC composite electrodes show fluctuations in CE; however, the HC composite electrode with 5% binder shows significant higher specific capacity compared to 2.5% and 10% binder. Note that the charging curves in Figure S8(a) indicate some problems with the stability of the cut off potential for the determination of the specific capacity, which was measured in the two-electrode cell versus the potential of the Na metal counter electrode. This problem was described in the literature.<sup>[69]</sup> It was also found that the addition of FEC could stabilize the Na metal electrode.<sup>[70,71]</sup> As a consequence in the presence of FEC, capacity fading is strongly diminished in accordance with our results (see Figures 3d and S8c). Capacity fading was slightly delayed for 5% binder but was for all three binder contents around the 25<sup>th</sup> cycle, which may be associated with inhomogeneous SEI layer formation that attenuates Na<sup>+</sup> ions insertion in HC in the following cycles.<sup>[70]</sup> Although the experimental conditions are not identical, Titirici and coworkers recently reported for solvothermally prepared HC in NaClO<sub>4</sub>/EC:DMC that decomposition products of the ClO<sub>4</sub><sup>-</sup> ions are incorporated into the basal plane of HC, which offers extra capacity for sodium storage. However, the capacity diminishes because of unstable adsorption of ClO<sub>4</sub><sup>-</sup> fragments, which subsequently exposes the carbon surface to continuous decomposition and subsequent sodium consumption.<sup>[72]</sup>

The HC composite electrode with 5% binder was also subjected to a longer cycling period of 100 cycles. The potential profiles of selected cycles, 1<sup>st</sup>, 2<sup>nd</sup>, 50<sup>th</sup> and 100<sup>th</sup> cycles are shown in Figure S8a. The capacity started to fade into two-fold reduced value (mAh g<sup>-1</sup>) after the 70<sup>th</sup> cycle. Although, there might be an issue with drift of the cut off potential for higher number of cycles which is also visible in Figure S8a after 50 cycles, we performed up to 100 cycles to evaluate the adherence of the spray-coated HC composite material on the Cu current collector. Capacity fading studies in Na half-cells for various electrolytes and HC materials have been reported. For example, hazelnut shell derived HC in 1 M NaPF<sub>6</sub> in EC:PC (1:1) showed capacity fading after the 50<sup>th</sup> cycle due to low reversibility of Na<sup>+</sup> ion storage for HC particles with highest impurities and highest amorphous carbon structure.<sup>[73]</sup> Half-cell studies, which are common in LIBs research have been initially adapted for SIBs employing HC anodes and Na metal cathodes.<sup>[61,74]</sup> However, it has been reported that for HC with Na metal lower rate capabilities have been obtained compared to full-cell studies.<sup>[60,69]</sup> Hence, our half-cell studies data are in line with half-cell studies reported in the literature. The stability/adhesion and the interfacial conductivity between the HC active material and the Cu current collector are important to prevent energy loss issues during long cycling tests. To overcome such issues, the current collector has to be pretreated<sup>[75]</sup> or the coating technique has to be optimized for good adhesion of active material. Figure S8(b) shows optical images

of the spray-coated composite HC electrodes (5 μm type II) before and after cycling, which reveal that there is no obvious delamination and hence, no significant loss of active material from the Cu current collector, even after 100 cycles. Hence the spray-coated HC composite electrode shows adequate adhesion and interfacial conductivity on the Cu current collector. In addition, the spray-coated HC electrodes were objected for 100 cycles in electrolyte containing FEC, as illustrated in Figure S8(c). The initial capacity decreased, but the capacity remains constant over 100 cycles.

The first discharge-charge galvanostatic cycling tests for 9 μm (type I and II) with 2.5%, 5% and 10% CMC binder are shown in Figure S9(a and b). The cycling performance varies among the different binder contents for the two different types (type I and type II) of 9 μm HC composite electrodes. HC composite electrodes (9 μm (type I)) with 2.5% binder show the highest capacity, whereas for 9 μm (type II) HC composite electrode with 5% binder show the highest capacity (Figure S9b). The difference in the cycling performance varies among the HC types, which seems to be associated with the lower moisture resistance of type I particles compared to type II HC particles (specification Kuranode HC, Kuraray).

The cycling performance of calendared spray-coated and DB HC composite electrodes during the first discharge-charge cycle are shown in Figure S9(c). The DB electrode shows slightly higher charging capacity in the first cycle when compared to the calendared electrode, potentially due to changes in the micro porosity of the composite after the calendaring process. However, the CE of both electrodes showed fluctuation over the investigated 50 cycles (also observed for the non-calendared HC composite electrode with 5% binder (Figure 3b). The specific capacity of both – the DB-coated HC composite electrode and the calendared, spray-coated HC composite electrode – are lower (69% and 22%, respectively for example at the 20<sup>th</sup> cycle) compared with the non-calendared electrode (5 μm, type II).

FEC has been used as additive for SIB half-cells and was shown to be a beneficial SEI-forming additive,<sup>[76]</sup> particularly when NaClO<sub>4</sub> in PC was used as electrolyte using layered NaNi<sub>0.5</sub>Mn<sub>0.5</sub>O<sub>2</sub> as cathode.<sup>[71]</sup> Based on the reports from the literature, the spray-coated electrodes were also investigated in presence of FEC during cycling (spray-coated HC with 5% binder) to evaluate the electrochemical performance (Figure 3c and d). As reported,<sup>[77]</sup> the current density (Figure 2b) and initial capacity in presence of FEC is decreased (Figure 3c), however, the capacity is about constant between 10<sup>th</sup> and 50<sup>th</sup> cycle (Figure 3d). In the first discharge-charge cycle, the plateau capacity is significantly decreased in presence of FEC when compared to the additive-free electrolyte. However, both specific capacity and CE maintain constant after the first few cycles until the 50<sup>th</sup> cycle. The initial CE of the HC composite in NaClO<sub>4</sub>/PC/2%FEC is lower. Despite that FEC leads to the formation of more stable SEI layers. The composition of the SEI in presence of FEC during cycling is rich in NaF (as shown in Figure 4). It has been shown that SEI layer with a higher content of NaF due to FEC as additive shows improved electrochemical behavior and better cycling performance.<sup>[70]</sup> Moreover, in

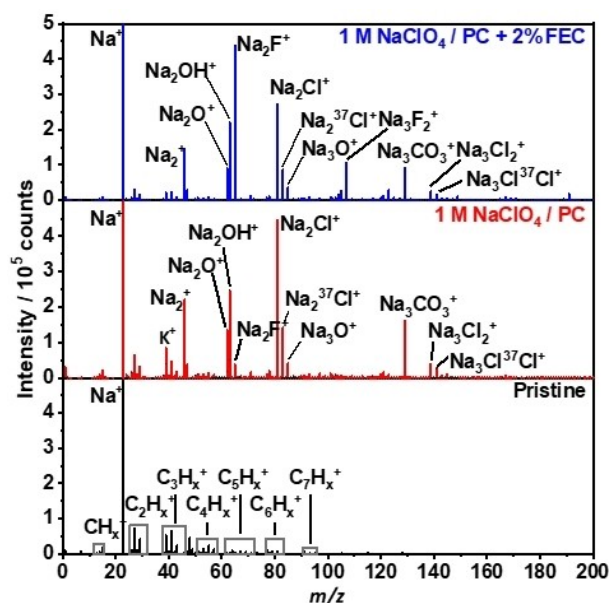


**Figure 4.** Exemplary ToF-SIMS surface spectra in positive secondary ion mode of the sample cycled in PC and 2% FEC (blue), the pristine sample (black) and the sample cycled in PC (red). The spectra are being displayed as line spectra with respect to the peak areas.

presence of FEC, a stable cathode electrolyte interphase (CEI) on the cathode side (Na metal) is formed. Our results correlate well with data from the literature.<sup>[77]</sup>

The capacity contribution during the discharge process has two regions:<sup>[78,79]</sup> the sloping region, above 0.25 V ( $\text{Na}^+$  ions adsorption) and the plateau region below 0.25 V ( $\text{Na}^+$  ions insertion), which were both investigated for the different HC composite electrodes in the first discharge-charge curve. The exact sodium storage mechanisms are still under debate.<sup>[59,76,80]</sup> The capacity distribution of the three different binder contents is illustrated in Figure S10.

The sloping region associated with  $\text{Na}^+$  ion adsorption of the composite electrodes with different binder content are similar (5  $\mu\text{m}$  (type II):  $215.25 \pm 32.04 \text{ mAh g}^{-1}$ ; 9  $\mu\text{m}$ , (type I):  $224.69 \pm 25.17 \text{ mAh g}^{-1}$  and 9  $\mu\text{m}$ , (type II):  $205.07 \pm 39.07 \text{ mAh g}^{-1}$ . For the obtained plateau region representing the  $\text{Na}^+$  ion insertion, only the 9  $\mu\text{m}$  (type I) containing electrode showed a lower capacity of  $138.36 \pm 15.28 \text{ mAh g}^{-1}$  compared to the electrodes with 5  $\mu\text{m}$  HC ( $180.86 \pm 13.34 \text{ mAh g}^{-1}$ ) and electrodes with 9  $\mu\text{m}$  HC (type II) ( $196.25 \pm 12.76 \text{ mAh g}^{-1}$ ). All measurements were obtained in triplicates. We also compared 5  $\mu\text{m}$  (type II) HC composite electrode with and without FEC with the calendared spray-coated and DB-coated composite electrodes (Figure S10b), which showed similar slope capacity contributions. However, the plateau capacity contribution is decreased for DB compared to the calendared spray-coated HC composite and HC composite electrodes cycled with the additive, indicating the adsorption (above 0.1 V) and  $\text{Na}^+$  ions insertion (below 0.1 V vs  $\text{Na}^+/\text{Na}$ ) into the HC, exhibiting a similar capacity contribution above 0.1 V.

Additionally, we determined the surface roughness of individual HC particles after cycling in 1 M  $\text{NaClO}_4$  in PC with and without FEC using AFM. It should be noted that a significantly smaller area compared to the initially performed  $S_a$  measurements with confocal laser microscopy was evaluated by the AFM measurements.  $S_a$  values of pristine and cycled (5 discharge-charge cycles) spray-coated HC electrodes are shown as bar diagram in Figure S13. As expected and known from LIBs,<sup>[81]</sup> an increase in  $S_a$  values of the HC composite electrodes after cycling is observed. The initial  $S_a$  value of  $192.8 \pm 25.81 \text{ nm}$  of pristine HC composite increased to  $310.0 \pm 19.3 \text{ nm}$  when cycled without FEC. A clear increase in  $S_a$  values was observed when the HC composite electrodes were cycled with FEC added to the electrolyte ( $404.6 \pm 67.6 \text{ nm}$ ). We associate this with the formation of a more inhomogeneous SEI layer<sup>[82]</sup> formed on the HC particle surface, as e.g. reported in 1 M  $\text{NaClO}_4$  in EC/PC(1:1).  $S_a$  analyses were also carried out for calendared spray-coated and DB-coated HC composite electrodes and the corresponding  $S_a$  values are shown in Figure S13b. Here, the  $S_a$  values show no significant changes before and after cycling.

Additionally, we conducted electrochemical impedance spectroscopy (EIS) to examine how the charge transfer resistance evolves after the initial 5 cycles. EIS was performed at OCP after the battery was rested for 8 h to ensure full wetting and after 5 cycles at the spray-coated HC (5  $\mu\text{m}$  type II) and DB-coated electrode to further investigate the effects of SEI growth along with structural and compositional changes. Generally, the semicircle of the Nyquist plots is related to the interfacial impedance of the HC composite electrode, which also contains contributions from the formation of SEI,<sup>[83–85]</sup> as shown in Figure S11.

An increase of the  $R_{\text{ct}}$  values after cycling was observed, which we associate with the formation of the SEI layer. The spray-coated HC composite electrode exhibited a larger interfacial resistance ( $R_{\text{SEI}} + R_{\text{ct}}$ ) of  $135.4 \Omega$  and the DB HC composite electrode of  $113.7 \Omega$  when compared to the pristine electrodes with OCP values of  $33.1 \Omega$  and  $31.2 \Omega$ , respectively. As a decreased specific capacity for spray-coated HC composite electrodes was observed in the first 5 cycles (Figure 3b, type II, 5%), we associate this with the increased resistance. The used equivalent circuit for classical SEI formation-resistance of an SEI layer is shown in Figure S12.<sup>[86]</sup>

### ToF-SIMS

To obtain mass spectrometric chemical information about the SEI layers, we ToF-SIMS measurements. For ToF-SIMS analysis, the sample surface is bombarded with a high energetic, low current pulsed primary ion-beam that ballistically sets free neutral particles, electrons, and ions of both polarities. The polarity-dependent, so-called secondary ions can be extracted by an appropriate electrical field and assigned by time-of-flight mass spectrometry. A detailed overview about the SIMS technique and its application in battery research is given in.<sup>[87]</sup>

Here we used ToF-SIMS for the characterization of the surface of pristine samples and SEIs formed on cycled spray-

coated HC composite electrodes (5 cycles in 1 M NaClO<sub>4</sub>/PC) with and without 2% FEC. Figure 4 shows exemplary mass spectra of the three sample types. Secondary ions, produced by ballistic impact that emerged from the surface of the pristine sample were mainly composed of hydrocarbon fragments next to the Na<sup>+</sup> fragment as can be seen in Figure 4 (bottom panel). The former can be regarded as contaminations by ambient atmosphere from the production and storage process, while the latter roots in the vast occurrence of Na<sup>+</sup> in natural samples, the precursor of the used HC, and from the Na-containing binder. The high Na<sup>+</sup> signal intensity is also related to its facile ionizability.

The surface of the cycled samples, either including (Figure 4, top panel) or excluding FEC (Figure 4, middle panel) showed the fragments Na<sub>2</sub>O<sup>+</sup>, Na<sub>2</sub>OH<sup>+</sup>, Na<sub>2</sub>Cl<sup>+</sup>, Na<sub>3</sub>CO<sub>3</sub><sup>+</sup> and Na<sub>2</sub>F<sup>+</sup>, respectively, as well as larger clusters and corresponding isotope derivatives. These ions can be associated to the chemical compounds Na<sub>2</sub>O, NaOH, NaCl, Na<sub>2</sub>CO<sub>3</sub> and additionally NaF when FEC was added to the electrolyte as additive. The named salts are typical compounds for the SEI of HC electrodes. Komaba et al. investigated the SEI layer on HC electrodes using PVDF as binder in Na<sup>+</sup> ion cells with pure PC electrolyte and 1 M NaClO<sub>4</sub> conductive salt, thus investigating SIB cells with comparable chemical composition as in this study.<sup>[46]</sup> The reported ToF-SIMS surface analysis revealed similar mass fragments, namely, Na<sub>2</sub>O<sup>+</sup>, Na<sub>2</sub>OH<sup>+</sup>, Na<sub>2</sub>Cl<sup>+</sup>, Na<sub>3</sub>CO<sub>3</sub><sup>+</sup>, Na<sub>2</sub>F<sup>+</sup> and the recombination product Na<sub>3</sub>FOH<sup>+</sup>. The oxides and hydroxides in both studies can be assigned to the degradation process of the conductive salt NaClO<sub>4</sub>. This hypothesis is substantiated by the detection of a compound including the remaining type of atom, Na<sub>2</sub>Cl<sup>+</sup>. The formation of carbonates like Na<sub>2</sub>CO<sub>3</sub> can be due to either the degradation of the electrolyte solvent PC or the additive FEC, with degradation of the latter also leading to the formation of the halide fragment Na<sub>2</sub>F<sup>+</sup>. Additional to the salt compounds, there are peaks of smaller intensity recognizable spread over the whole mass range that is depicted in Figure 4 (cycled samples). These correspond to organic products from electrolyte degradation, which are obviously minor compounds since the ionisation probability of positive organic mass fragments is usually quite high.

In the literature, it is broadly accepted that in contrast to the organic-rich SEI in LIBs, the SEI in SIBs is composed of inorganic salts, while organic compounds make out only minor contribution to the functionality of the SEI layer.<sup>[46]</sup> Partly, this can be attributed to the fact that the sum of the detected chemical compounds carbonate and fluoride do not yet add up to portray the whole molecules of PC or FEC, respectively. Further carbonaceous decomposition products could be expected, which would lead to higher intensity peaks. The missing species composed of the alkylene backbone of the used solvent evade in the form of gaseous components, like ethene and propene, as was shown by online electrochemical mass spectrometry (OEMS)<sup>[88]</sup> and hence, are not available for the formation of organic moieties building the SEI.

Further noticeable is the intensity ratio of the signals stemming from the halide NaCl (Na<sub>2</sub>Cl<sup>+</sup> and Na<sub>3</sub>Cl<sub>2</sub><sup>+</sup>), oxide Na<sub>2</sub>O and hydroxide NaOH, respectively (Na<sub>2</sub>O<sup>+</sup>, Na<sub>2</sub>OH<sup>+</sup>).

Comparing the additive-free sample and additive-containing sample, the relative intensity of the Na<sub>2</sub>Cl<sup>+</sup>-fragment was decreased compared to the intensity of the Na<sub>2</sub>O<sup>+</sup>-fragment. The switch of the intensity ratio cannot be attributed to the concentration of the chlorine containing conductive salt NaClO<sub>4</sub>, which was equal in both samples. This effect might arise due to the reaction of fluoride being favored over the reaction of chloride during SEI formation.

The presented results are limited to the surface area of the samples for the intrinsic surface sensitivity of the analytical method, which is about a few nanometres. Despite the reliability of the SIMS method itself, we cannot exclude that during the necessary cleaning step after cycling (rinsing) parts of the surface, salts may have been washed off the sample, and hence could not be detected anymore. However, the here-shown investigations of cycled half-cell SIB in the light of the addition of FEC hints a clear impact to the formation of the binary halide NaF.

### Pulsed charging and thermal behavior of HC films

Figure 5 shows the behavior of a 20 μm thick HC composite film upon pulsed discharging/charging with 10 ms positive and negative current pulses (Figures 5a and b; black line) with a 300 μA amplitude. This current amplitude corresponds to a discharging/charging rate of about 3 C with a geometrical area of the sample of ca. 0.2 cm<sup>2</sup>. The equilibrium potential before the pulse is 60 mV and corresponds to a state of charge of approximately 70%.

The potential (blue line) steeply rises/falls by about 60 mV with the initial current step. During the pulse, it continues to change and no steady overpotential is reached. At the end of the external current flow the potential immediately jumps to a value about 10 mV positive/negative of the starting potential,

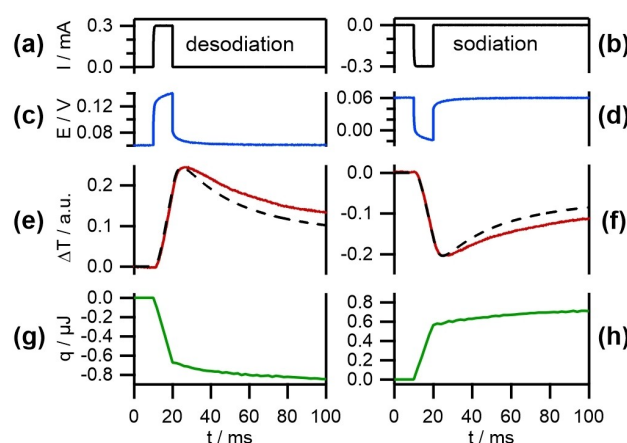


**Figure 5.** Current (black), potential (blue), temperature (red), and heat (green) transients upon pulsed discharging (a, c, e, g) and charging (b, d, f, h) of a 20 μm thick HC film by 10 ms positive and negative current pulses with 300 μA amplitude, respectively. In addition, the thermal response of the electrode to a 10 ms laser pulse is shown as a black dashed line. The amplitude is adjusted to the extremum of the respective temperature transient.

indicating an IR drop in the three-electrode cell of about 60 mV. After the pulses the potential quickly relaxes towards the starting potential within about 10 ms. Possible reasons for the potential relaxation without external current flow may be equilibration of Na concentration gradients inside the HC grains and the electrolyte or discharging of the double layer by sluggish Na<sup>+</sup> ion insertion/extraction at the electrode-electrolyte interface. Since we changed the state of charge of the working electrode by merely about 0.01% by the short current pulses, we expect only small concentration gradients. We therefore rather attribute the electrochemical relaxation to sluggish charge transfer kinetics and double layer discharging.

The thermal response of the HC film to the discharging/charging pulses is shown in Figure 5(e) and (f), respectively. The temperature of the HC electrode is measured at its backside with a thin pyroelectric sensor. The total thickness of the electrode-sensor assembly is about 100 μm, ensuring fast thermal equilibration between HC electrode and sensor (see experimental section). Upon discharging (desodiation) the electrode temperature starts to rise about linearly with a delay of about 1 ms after the beginning of the current pulse. After the end of the pulse the temperature reaches a maximum about 7 ms after the end of the current pulse, before the temperature relaxes towards the starting temperature on a time scale of several 100 ms by heat dissipation into the surrounding. In addition to the electrochemically driven temperature transients in Figures 5(e and f), also the thermal response function following the heat uptake from irradiation of the front side of the HC-film by a 10 ms laser pulse is shown as dashed line. The laser temperature-transient was recorded in the same experiment. Its amplitude was adjusted to that of the electrochemical temperature response for better comparability. The thermal response of the electrode to laser irradiation increases about linearly from the beginning of the laser pulse, also with a delay of 1 ms similar to the response from the electrochemical reaction. This indicates fast heat transport through the HC-film and the electrode. Indeed, the maximum temperature upon laser irradiation is reached only 4 ms after the irradiation stopped, followed by a rather fast decay during temperature equilibration. The electrochemically driven temperature transients relax considerably slower than the purely thermal response, signaling that there is significant heat evolution also in the absence of external current flow through the cell. In Figure 5(g and h), we show the heat as a function of time, as it is reconstructed from the temperature signals by deconvolution with the thermal response function of the calorimeter.<sup>[89]</sup> From the heat transients it can be clearly seen that although most of the heat is evolved during the current pulse, heat evolution continued up to about 400 ms after the pulse without external current flow, extending much beyond the time scale of the electrochemical equilibration, seen in Figure 5(c and d).

By comparison of the left and right column of Figure 5, it can be directly conceived that the potential response to the current pulse as well as the thermal responses of the HC electrode almost quantitatively revert upon changing the pulse polarity. This indicates high reversibility of the sodiation/desodiation process under the applied conditions with minute

conversions. The heat exchanged reversibly at an electrode upon an electrochemical reaction can be identified with the entropy change during the reaction.<sup>[90,91]</sup> From the sign of temperature change, we find positive reaction entropy for the charging process, which is in accordance with entropy gain upon the release of solvent molecules from the solvation shell upon the sodiation of the HC composite electrode. This is similar to the results upon bulk deposition of lithium or sodium.<sup>[44,92]</sup> We estimate that reaction entropies for Na bulk deposition and Na insertion into HC are of the same order of magnitude, which is in accordance with recent findings.<sup>[59]</sup> From the sign of temperature change, we find positive reaction entropy for the charging process for the probed SoC of about 70%. Quantitative evaluation of the data yielded approximately 80 J mol<sup>-1</sup> K<sup>-1</sup> at  $t=400$  ms, which comes close to the value for Na metal-deposition from NaClO<sub>4</sub>/PC solution (83 J mol<sup>-1</sup> K<sup>-1</sup>).<sup>[93]</sup> This is in agreement with results from entropy profiling of half-cells reported in the literature,<sup>[94]</sup> where only small differences between metal-deposition and sodiation entropies at high SoC were reported. The positive reaction entropy upon Na insertion or deposition is readily explained by the entropy gain upon the release of solvent molecules from the solvation shell, which overcompensates entropy losses due to fixation of Na<sup>+</sup> ions and which was similarly observed for Li deposition.<sup>[44,92]</sup> SoC-dependent measurements of the entropy of the sodiation of HC may yield variations of the configurational entropy of the Na in the HC composite and thus may reveal a more detailed picture of the involved processes. Such investigations are within reach, due to the thin, thermally well conductive spray-coated HC electrodes.

## Conclusions

The spray-coating technique is a versatile method for preparing HC composite anodes with different particle sizes and binder contents tailored in the presented case specifically for Na<sup>+</sup> ion storage. In this study, HC composite electrodes with different HC particle sizes and binder contents (2.5%, 5%, and 10% CMC) were prepared with controlled thickness and mass loading. These HC composite anodes were then investigated in respect to coulombic efficiency and specific capacity and characterized in terms of physical properties like surface roughness and active mass loading. The electrochemical performance and the stability of SEI has been investigated and associated with the surface reactivity and cycling stability for HC composite electrodes with 5 μm (type II) HC particles. Notably, the results revealed distinct surface reactivity of the spray-coated HC composite electrodes towards SEI formation in 1 M NaClO<sub>4</sub> in PC leading to capacity changes, which were found to be dependent on used HC and binder composition as well as applied electrolyte additive.

We observed differences in the capacity contribution for spray-coated HC electrodes compared to DB-coated HC composite electrodes. We assume that these differences in the slope and plateau region are due to different pore networks and HC arrangements resulting from fabrication processes. ToF-SIMS

measurements revealed the evolution of SEI layer components in both additive-free and additive-containing electrolyte. The spray-coating proves its efficacy in producing HC films, notably thin in nature, with rapid electrochemical and thermal responses making them highly suitable for utilization in microcalorimetry experiments. Future studies will evaluate spray-coating also for cathode materials, avoiding Na metal in half-cell experiments, focusing on a comprehensive study on SEI/CEI formation/composition in different electrolyte salt/solvent mixtures.

## Experimental Section

### Materials and chemicals

The electrolyte was prepared by mixing 1 M NaClO<sub>4</sub> (Alfa Aesar, Germany) and anhydrous propylene carbonate (Sigma Aldrich, Germany). For studies with additives 4-Fluoro-1,3-dioxolan-2-one (FEC, 2 v/v) (Sigma Aldrich, Germany) was added. HC active materials was obtained from Kuraray (Kuranode, 9 μm (type I), 5 μm (type II) and 9 μm (type II), Japan). Carbon black was purchased from Cabot Corporation (Vulcan XC72R, USA) and sodium carboxymethyl cellulose (CMC, molecular weight ~124000) was purchased from Sigma Aldrich, Germany.

### Electrode fabrication by spray-coating

Na-based CMC was dissolved in water (18 MΩcm) for 30 min at 50 °C. CC (10%) and HC with different particle sizes (5 μm (type II), 9 μm (type I) and 9 μm (type II)) were mixed in the corresponding ratio and added to the CMC solution. After stirring the solution for 48 h at 50 °C isopropyl alcohol (IPA) was added. The spray gun was filled with the slurry and moved perpendicular to the substrate electrode (a copper foil), while a distance of 15 cm between the spray nozzle and surface was kept constant. Electrodes were prepared with different percentages of CMC ranging from 2.5% to 10%. The spray-coated electrodes were dried overnight at RT and then vacuum dried at 80 °C for 12 h. One batch of the spray-coated electrodes was calendared with a compression of 1000 kg (TOB-NL-12, TOB New Energy Technology, China).

### Characterization of spray-coated HC electrodes

Thickness and surface roughness of the spray-coated electrodes were characterized by 3D laser scanning microscopy (VK-X3000, Keyence, Japan). Surface morphology and arrangement of HC particles within the spray-coated electrodes were analyzed by focused ion beam-scanning electron microscopy (FIB/SEM) (Quanta 3D FEG, ThermoFisher Scientific, the Netherlands). Raman spectroscopy was carried out using a confocal Raman microspectrometer (InVia QONTOR, Renishaw, United Kingdom) with a red laser at 748 nm and a 20× objective lens in back-scatter configuration. A spectrum was collected in the range of 100–3500 cm<sup>-1</sup> with a resolution of 0.7 cm<sup>-1</sup> (10 accumulations of 5 s) and was processed with background removal and normalization. The d-spacing of HC particles was analyzed by X-ray diffraction (XRD) measurements using an X-ray diffractometer (STOE – Stadi P, STOE, Germany) equipped with an Ag K<sub>α</sub> radiation source (λ = 0.55941 Å) in transmission mode.

### Electrochemical tests

HC composite anodes with a loading density of 1.82 ± 0.23 mg cm<sup>-2</sup> (n = 3, (5 μm, type II)), 2.32 ± 0.47 mg cm<sup>-2</sup> (n = 3, (9 μm, type I)) and 1.45 ± 0.18 mg cm<sup>-2</sup> (n = 3, (9 μm, type II)) were prepared and mounted in a Swagelok cell assembled in an Ar-filled glovebox (Unilab, MBraun, Germany, O<sub>2</sub> < 0.1 ppm and H<sub>2</sub>O < 0.1 ppm) in a two-electrode configuration using sodium as cathode and a glass-fiber separator (Whatman GF/F, United Kingdom). Electrochemical tests were performed using a battery testing station (Biologic BS-805, Biologic, France) at RT in galvanostatic mode between 0.01 and 2.00 V vs. Na<sup>+</sup>/Na at 20 mA g<sup>-1</sup>. The same setup was used to perform CV to investigate the reduction and oxidation peaks in the voltage range of 0.01–2.00 V vs. Na<sup>+</sup>/Na at a scan rate of 0.1 mV s<sup>-1</sup>. EIS was performed in the frequency range of 10 kHz to 10 mHz with a perturbation amplitude of 5 mV under no-bias conditions using the same battery testing system.

### SEI layer analysis

AFM measurements were carried out using an atomic force microscope (Park NX10, Park Systems, South Korea) located in a glovebox (Unilab, MBraun, Germany) in an argon atmosphere (O<sub>2</sub> < 0.1 ppm and H<sub>2</sub>O < 0.1 ppm). AFM probes (PPP-NCL, Nanosensors, Switzerland) with a resonant frequency of 190 kHz, a nominal tip radius of < 10 nm and a nominal spring constant of 48 N m<sup>-1</sup> were used as the probe to map the surface morphology and to determine the surface roughness of cycled HC electrodes in non-contact mode at a scan speed of 0.5 Hz. A high-frequency cantilever was operated exclusively in the attractive force regime. The force constant of each cantilever was determined prior to the measurement using the thermal noise method.<sup>[95]</sup> The AFM images were analyzed using an imaging processing tool for SPM data (XEI 5.2, Park Systems, South Korea). Roughness parameters before and after cycling obtained by AFM were calculated from 5 × 5 μm (5 μm (type II) areas (five different spots of one sample (512 × 512 pixel))).

### Time-of-flight secondary ion mass spectrometry (ToF-SIMS)

For the different types of electrodes (pristine, cycled with and without FEC) 5 spots on 3 electrodes of each group were analyzed by static ToF-SIMS in positive ion mode by using a ToF-SIMS 5–100 instrument (IONTOF GmbH, Germany), which was equipped with a 25 keV Bi cluster primary ion source. For analysis, a pulsed Bi<sup>+</sup> primary ion beam was scanned over a surface area of 50 μm × 50 μm with 128 × 128 pixels until a dose density of 2.60 × 10<sup>13</sup> ions cm<sup>-2</sup> was reached at a cycle time of 100 μs. Charge compensation was carried out with a low energetic electron gun. The achieved mass resolution was better than  $m/\Delta m = 3000$  (FWHM) at  $m/z$  64.98 (Na<sub>2</sub>F<sup>+</sup>). For data analysis SurfaceLab (version 7.2, IONTOF GmbH, Germany) was used by which the surface spectra were calibrated to the peaks of the fragments CH<sub>3</sub><sup>+</sup>, C<sub>2</sub>H<sub>3</sub><sup>+</sup>, C<sub>3</sub>H<sub>5</sub><sup>+</sup>, C<sub>4</sub>H<sub>7</sub><sup>+</sup>, C<sub>6</sub>H<sub>9</sub><sup>+</sup> and C<sub>7</sub>H<sub>8</sub><sup>+</sup>.

### Microcalorimetry

The potential, temperature, and heat response of the HC composite films to the charging/discharging pulses was analyzed in 1 M NaClO<sub>4</sub> in PC with 2% FEC additive by single electrode microcalorimetry. The home-built setup consisted of a customized PEEK cell (V = 0.5 mL) with its working electrode (A = 0.2 cm<sup>2</sup>) directly mounted on a pyroelectric sensor.<sup>[96]</sup> Na wires (Ø = 1 mm) were used as reference and counter electrodes. The three electrodes were connected to a home-built potentiostat. For further exper-

imental details see, e.g., reference<sup>[93]</sup> Data acquisition and evaluation was performed with Wavemetrics Igor Pro 9.

## Supporting information

The authors have cited additional references within the Supporting Information.<sup>[97]</sup>

## Acknowledgements

The Focused Ion Beam Center UUlM and Gregor Neusser are acknowledged. We thank Prof. Dr. Boris Mizaikoff (Hahn-Schickard, Ulm) for the possibility to use the 3D laser scanning microscopy. This work contributes to the research performed at CELEST (Center for Electrochemical Energy Storage Ulm – Karlsruhe) and was funded by the Deutsche Forschungsgemeinschaft (DFG, German Research Foundation) under Germany's Excellence Strategy – EXC 2154 – Project number 390874152 (POLIS Cluster of Excellence). Open Access funding enabled and organized by Projekt DEAL.

## Conflict of Interests

The authors declare that they have no known competing financial interests or personal relationships that could have appeared to influence the work reported in this paper.

## Data Availability Statement

The data that support the findings of this study are openly available at Zenodo at DOI: 10.5281/zenodo.8344722, reference number [98].

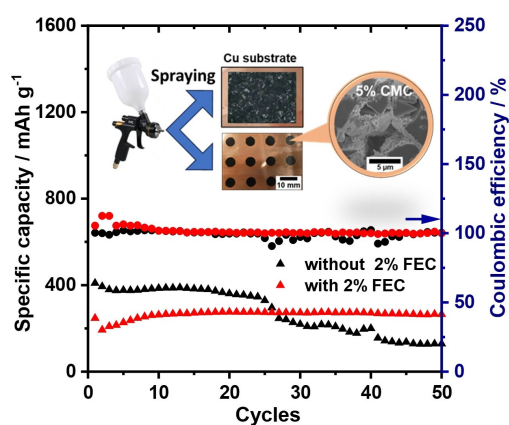
**Keywords:** spray-coating · hard carbon · intercalation · SEI layer · sodium-ion batteries

- [1] P. Haidl, A. Buchroithner, B. Schweighofer, M. Bader, H. Wegleiter, *Sustainability* **2019**, *11*, 6731.
- [2] V. Palomares, P. Serras, I. Villaluenga, K. B. Hueso, J. Carretero-González, T. Rojo, *Energy Environ. Sci.* **2012**, *5*, 5884.
- [3] C. Vaalma, D. Buchholz, S. Passerini, *Curr. Opin. Electrochem.* **2018**, *9*, 41–48.
- [4] D. A. Stevens, J. R. Dahn, *J. Electrochem. Soc.* **2000**, *147*, 1271.
- [5] E. Irisarri, A. Ponrouch, M. R. Palacin, *J. Electrochem. Soc.* **2015**, *162*, A2476–A2482.
- [6] J. Song, B. Xiao, Y. Lin, K. Xu, X. Li, *Adv. Energy Mater.* **2018**, *8*, 1–24.
- [7] C. Nita, B. Zhang, J. Dentzer, C. Matei Ghimbeu, *J. Energy Chem.* **2021**, *58*, 207–218.
- [8] T.-L. T. Thu, T.-L. T. Thu, T. D. Manh, T.-T. Tan, J.-K. Chang, *J. Mater. Res. Technol.* **2021**, *13*, 1139–1149.
- [9] J. Du, W. Wang, M. Wan, X. Wang, G. Li, Y. Tan, C. Li, S. Tu, Y. Sun, *Adv. Energy Mater.* **2021**, *11*, 1–10.
- [10] S. H. Lee, K. Li, C. Huang, J. D. Evans, P. S. Grant, *ACS Appl. Mater. Interfaces* **2019**, *11*, 603–612.
- [11] Y. Liu, X. Gong, C. Podder, F. Wang, Z. Li, J. Liu, J. Fu, X. Ma, P. Vanaphuti, R. Wang, A. Hitt, Y. Savsatli, Z. Yang, M. Ge, W.-K. Lee, B. Yonemoto, M. Tang, H. Pan, Y. Wang, *Joule* **2023**, *7*, 952–970.

- [12] C. C. Lalau, C. T. J. Low, *Batteries & Supercaps* **2019**, *2*, 551–559.
- [13] S. C. Lee, J. Jeong, H. G. Park, B. C. Min, S. Chan Jun, K. Y. Chung, *J. Power Sources* **2020**, *472*, 228573.
- [14] R. Yu, Y. Sun, B. K. Zou, M. M. Deng, J. Y. Xie, C. H. Chen, *J. Power Sources* **2017**, *340*, 258–262.
- [15] D. Liu, L. C. Chen, T. J. Liu, W. B. Chu, C. Tiu, *Energy Technol.* **2017**, *5*, 1235–1241.
- [16] C. C. Ho, K. Murata, D. A. Steingart, J. W. Evans, P. K. Wright, *J. Micromech. Microeng.* **2009**, *19*, 094013.
- [17] L. A. Román-Ramírez, G. Apachitei, M. Faraji-Niri, M. Lain, W. D. Widanage, J. Marco, *J. Power Sources* **2021**, *516*, 230689.
- [18] Y. Zhang, F. Huld, S. Lu, C. Jektvik, F. Lou, Z. Yu, *Batteries* **2022**, *8*, 57.
- [19] J. E. Bishop, J. A. Smith, D. G. Lidzey, *ACS Appl. Mater. Interfaces* **2020**, *12*, 48237–48245.
- [20] M. A. Garakani, S. Bellani, V. Pellegrini, R. Oropesa-Nuñez, A. E. D. R. Castillo, S. Abouali, L. Najafi, B. Martín-García, A. Ansaldo, P. Bondavalli, C. Demirci, V. Romano, E. Mantero, L. Marasco, M. Prato, G. Bracciale, F. Bonaccorso, *Energy Storage Mater.* **2021**, *34*, 1–11.
- [21] G. G. Eshetu, G. A. Elia, M. Armand, M. Forsyth, S. Komaba, T. Rojo, S. Passerini, *Adv. Energy Mater.* **2020**, *10*, 2000093.
- [22] K. Pfeifer, S. Arnold, J. Becherer, C. Das, J. Maibach, H. Ehrenberg, S. Dsoke, *ChemSusChem* **2019**, *12*, 3312–3319.
- [23] P. Barnes, K. Smith, R. Parrish, C. Jones, P. Skinner, E. Storch, Q. White, C. Deng, D. Karsann, M. L. Lau, J. J. Dumais, E. J. Dufek, H. Xiong, *J. Power Sources* **2020**, *447*, 227363.
- [24] J. Pan, Y. Sun, Y. Yan, L. Feng, Y. Zhang, A. Lin, F. Huang, J. Yang, *JACS Au* **2021**, *1*, 1208–1216.
- [25] K. Wang, Y. Xu, Y. Li, V. Dravid, J. Wu, Y. Huang, *J. Mater. Chem. A* **2019**, *7*, 3327–3335.
- [26] H. S. Hirsh, B. Sayahpour, A. Shen, W. Li, B. Lu, E. Zhao, M. Zhang, Y. S. Meng, *Energy Storage Mater.* **2021**, *42*, 78–87.
- [27] E. Wang, Y. Niu, Y. X. Yin, Y. G. Guo, *ACS Materials Lett.* **2021**, *3*, 18–41.
- [28] S. L. Chou, Y. Pan, J. Z. Wang, H. K. Liu, S. X. Dou, *Phys. Chem. Chem. Phys.* **2014**, *16*, 20347–20359.
- [29] J. Li, R. B. Lewis, J. R. Dahn, *Electrochem. Solid-State Lett.* **2007**, *10*, A17.
- [30] M. Dahbi, T. Nakano, N. Yabuuchi, T. Ishikawa, K. Kubota, M. Fukunishi, S. Shibahara, J. Y. Son, Y. T. Cui, H. Oji, S. Komaba, *Electrochem. Commun.* **2014**, *44*, 66–69.
- [31] Z. Yang, J. He, W. H. Lai, J. Peng, X. H. Liu, X. X. He, X. F. Guo, L. Li, Y. Qiao, J. M. Ma, M. Wu, S. L. Chou, *Angew. Chem. Int. Ed.* **2021**, *60*, 27086–27094.
- [32] C. Bommier, X. Ji, *Small* **2018**, *14*, 1–20.
- [33] D. Bresser, D. Buchholz, A. Moretti, A. Varzi, S. Passerini, *Energy Environ. Sci.* **2018**, *11*, 3096–3127.
- [34] M. Singh, J. Kaiser, H. Hahn, *J. Electrochem. Soc.* **2015**, *162*, A1196–A1201.
- [35] D. Devaux, H. Leduc, P. Dumaz, M. Lecuyer, M. Deschamps, R. Bouchet, *Front. Energy Res.* **2020**, *7*, 1–10.
- [36] G. Yang, I. N. Ivanov, R. E. Ruther, R. L. Sacci, V. Subjakova, D. T. Hallinan, J. Nanda, *ACS Nano* **2018**, *12*, 10159–10170.
- [37] S. H. Lapidus, N. N. Rajput, X. Qu, K. W. Chapman, K. A. Persson, P. J. Chupas, *Phys. Chem. Chem. Phys.* **2014**, *16*, 21941–21945.
- [38] M. Wang, Q. Wang, X. Ding, Y. Wang, Y. Xin, P. Singh, F. Wu, H. Gao, *Interdiscip. Mater.* **2022**, *1*, 373–395.
- [39] H. Wang, F. Liu, R. Yu, J. Wu, *Interdiscip. Mater.* **2022**, *1*, 196–212.
- [40] X. Liu, X. Jiang, Z. Zeng, X. Ai, H. Yang, F. Zhong, Y. Xia, Y. Cao, *ACS Appl. Mater. Interfaces* **2018**, *10*, 38141–38150.
- [41] Y. Kim, K. H. Ha, S. M. Oh, K. T. Lee, *Chem. Eur. J.* **2014**, *20*, 11980–11992.
- [42] D. Karabelli, S. Singh, S. Kiemel, J. Koller, A. Konarov, F. Stubhan, R. Mieke, M. Weeber, Z. Bakonov, K. P. Birke, *Front. Energy Res.* **2020**, *8*, 1–16.
- [43] J. Asenbauer, A. Wirsching, M. Lang, S. Indris, T. Eisenmann, A. Mullaliu, A. Birrozzi, A. Hoefling, D. Geiger, U. Kaiser, R. Schuster, D. Bresser, *Adv. Sustainable Syst.* **2022**, *6*, 2200102.
- [44] M. J. Schmid, K. R. Bickel, P. Novák, R. Schuster, *Angew. Chem. Int. Ed.* **2013**, *52*, 13233–13237.
- [45] J. Meng, G. Jia, H. Yang, M. Wang, *Front. Chem.* **2022**, *10*, 1–7.
- [46] S. Komaba, W. Murata, T. Ishikawa, N. Yabuuchi, T. Ozeki, T. Nakayama, A. Ogata, K. Gotoh, K. Fujiwara, *Adv. Funct. Mater.* **2011**, *21*, 3859–3867.
- [47] M. Carboni, J. Manzi, A. R. Armstrong, J. Billaud, S. Brutti, R. Younesi, *ChemElectroChem* **2019**, *6*, 1745–1753.
- [48] Y. Li, W. Huang, Y. Li, A. Pei, D. T. Boyle, Y. Cui, *Joule* **2018**, *2*, 2167–2177.
- [49] B. Han, Y. Zou, Z. Zhang, X. Yang, X. Shi, H. Meng, H. Wang, K. Xu, Y. Deng, M. Gu, *Nat. Commun.* **2021**, *12*, 1–8.

- [50] S. Daboss, T. Philipp, K. Palanisamy, J. Flowers, H. S. Stein, C. Kranz, *Electrochim. Acta* **2023**, *453*, 142345.
- [51] J. H. Park, S. H. Kim, K. H. Ahn, *Colloids Surf. A* **2023**, *664*, 131130.
- [52] Z. Lin, T. Liu, X. Ai, C. Liang, *Nat. Commun.* **2018**, *9*, 5262.
- [53] X. Dou, I. Hasa, D. Saurel, C. Vaalma, L. Wu, D. Buchholz, D. Bresser, S. Komaba, S. Passerini, *Mater. Today* **2019**, *23*, 87–104.
- [54] A. Beda, F. Rabuel, M. Morcrette, S. Knopf, P. L. Taberna, P. Simon, C. Matei Ghimbeu, *J. Mater. Chem. A* **2021**, *9*, 1743–1758.
- [55] R. Gond, H. D. Asfaw, O. Hosseinaei, K. Edström, R. Younesi, A. J. Naylor, *ACS Sustainable Chem. Eng.* **2021**, *9*, 12708–12717.
- [56] Z. V. Bobyleva, O. A. Drozhzhin, K. A. Dosaev, A. Kamiyama, S. V. Ryazantsev, S. Komaba, E. V. Antipov, *Electrochim. Acta* **2020**, *354*, 136647.
- [57] N. Soltani, A. Bahrami, L. Giebeler, T. Gemming, D. Mikhailova, *Prog. Energy Combust. Sci.* **2021**, *87*, 100929.
- [58] M. S. Balogun, Y. Luo, W. Qiu, P. Liu, Y. Tong, *Carbon* **2016**, *98*, 162–178.
- [59] M. P. Mercer, S. Affleck, E. M. Gavilán-Arriazu, A. A. Zülke, P. A. Maughan, S. Trivedi, M. Fichtner, A. Reddy Munnangi, E. P. M. Leiva, H. E. Hoster, *ChemPhysChem* **2022**, *23*, e202100748.
- [60] X. Chen, Y. Zheng, W. Liu, C. Zhang, S. Li, J. Li, *Nanoscale* **2019**, *11*, 22196–22205.
- [61] J. M. Stratford, P. K. Allan, O. Pecher, P. A. Chater, C. P. Grey, *Chem. Commun.* **2016**, *52*, 12430–12433.
- [62] A. Hofmann, Z. Wang, S. P. Bautista, M. Weil, F. Müller, R. Löwe, L. Schneider, I. U. Mohsin, T. Hanemann, *Electrochim. Acta* **2022**, *403*, 139670.
- [63] F. S. Genier, S. Pathreker, R. L. Schuarca, M. Islam, I. D. Hosein, *ECS Adv.* **2022**, *1*, 030502.
- [64] D. A. Stevens, J. R. Dahn, *J. Electrochem. Soc.* **2001**, *148*, A803.
- [65] L. Pei, H. Cao, L. Yang, P. Liu, M. Zhao, B. Xu, J. Guo, *Ionics* **2020**, *26*, 5535–5542.
- [66] M. Ma, H. Cai, C. Xu, R. Huang, S. Wang, H. Pan, Y. Hu, *Adv. Funct. Mater.* **2021**, *31*, 2100278.
- [67] H. Dong, R. Liu, X. Hu, F. Zhao, L. Kang, L. Liu, J. Li, Y. Tan, Y. Zhou, D. J. L. Brett, G. He, I. P. Parkin, *Adv. Sci.* **2023**, *10*, 1–12.
- [68] A. Mistry, S. Trask, A. Dunlop, G. Jeka, B. Polzin, P. P. Mukherjee, V. Srinivasan, *J. Electrochem. Soc.* **2021**, *168*, 070536.
- [69] Z. Li, Z. Jian, X. Wang, I. A. Rodríguez-Pérez, C. Bommier, X. Ji, *Chem. Commun.* **2017**, *53*, 2610–2613.
- [70] J. Fondard, E. Irisarri, C. Courrèges, M. R. Palacin, A. Ponrouch, R. Dedryvère, *J. Electrochem. Soc.* **2020**, *167*, 070526.
- [71] S. Komaba, T. Ishikawa, N. Yabuuchi, W. Murata, A. Ito, Y. Ohsawa, *ACS Appl. Mater. Interfaces* **2011**, *3*, 4165–4168.
- [72] H. Alptekin, H. Au, E. Olsson, J. Cottom, A. C. Jensen, T. F. Headen, Q. Cai, A. J. Drew, M. Crespo Ribadeneyra, M. Titirici, *Adv. Mater. Interfaces* **2022**, *9*, 2101267.
- [73] H. Moon, A. Innocenti, H. Liu, H. Zhang, M. Weil, M. Zarrabeitia, S. Passerini, *ChemSusChem* **2023**, *16*, e202201713.
- [74] A. R. Shah, R. R. C. Shutt, K. Smith, J. Hack, T. P. Neville, T. F. Headen, D. J. L. Brett, C. A. Howard, T. S. Miller, P. L. Cullen, *J. Phys. Mater.* **2021**, *4*, 042008.
- [75] N. Sun, Q. Zhu, B. Anasori, P. Zhang, H. Liu, Y. Gogotsi, B. Xu, *Adv. Funct. Mater.* **2019**, *29*, 1906282.
- [76] M. Anji Reddy, M. Helen, A. Groß, M. Fichtner, H. Euchner, *ACS Energy Lett.* **2018**, *3*, 2851–2857.
- [77] A. Ponrouch, A. R. Goñi, M. R. Palacin, *Electrochem. Commun.* **2013**, *27*, 85–88.
- [78] S. Qiu, L. Xiao, M. L. Sushko, K. S. Han, Y. Shao, M. Yan, X. Liang, L. Mai, J. Feng, Y. Cao, X. Ai, H. Yang, J. Liu, *Adv. Energy Mater.* **2017**, *7*, 1–11.
- [79] N. Sun, Z. Guan, Y. Liu, Y. Cao, Q. Zhu, H. Liu, Z. Wang, P. Zhang, B. Xu, *Adv. Energy Mater.* **2019**, *9*, 1–14.
- [80] X. Chen, C. Liu, Y. Fang, X. Ai, F. Zhong, H. Yang, Y. Cao, *Carbon Energy* **2022**, *4*, 1133–1150.
- [81] L. Y. Beaulieu, A. D. Rutenberg, J. R. Dahn, *Microsc. Microanal.* **2002**, *8*, 422–428.
- [82] H. Lohani, A. Kumar, P. Kumari, A. Ahuja, M. Gautam, A. Sengupta, S. Mitra, *ACS Appl. Mater. Interfaces* **2022**, *14*, 37793–37803.
- [83] F. Linsenmann, D. Pritzl, H. A. Gasteiger, *J. Electrochem. Soc.* **2019**, *166*, A3668–A3674.
- [84] R. Väli, A. Jänes, E. Lust, *J. Electrochem. Soc.* **2017**, *164*, E3429–E3437.
- [85] Z. Chen, H. Duan, Z. Xu, C. Chen, Y. Yan, S. Wu, *Adv. Mater. Interfaces* **2020**, *7*, 1–10.
- [86] V. A. Nikitina, M. V. Zakharkin, S. Y. Vassiliev, L. V. Yashina, E. V. Antipov, K. J. Stevenson, *Langmuir* **2017**, *33*, 9378–9389.
- [87] T. Lombardo, F. Walther, C. Kern, Y. Moryson, T. Weintraut, A. Henss, M. Rohnke, *J. Vac. Sci. Technol. A* **2023**, *41*, 053207.
- [88] L. Zhang, C. Tsolakidou, S. Mariyappan, J. M. Tarascon, S. Trabesinger, *Energy Storage Mater.* **2021**, *42*, 12–21.
- [89] K. R. Bickel, K. D. Etzel, V. Halka, R. Schuster, *Electrochim. Acta* **2013**, *112*, 801–812.
- [90] T. Ozeki, N. Ogawa, K. Aikawa, I. Watanabe, S. Ikeda, *J. Electroanal. Chem.* **1983**, *145*, 53–65.
- [91] R. Schuster, *Curr. Opin. Electrochem.* **2017**, *1*, 88–94.
- [92] M. J. Schmid, J. Xu, J. Lindner, P. Novák, R. Schuster, *J. Phys. Chem. B* **2015**, *119*, 13385–13390.
- [93] F. Karcher, M. Uhl, T. Geng, T. Jacob, R. Schuster, *Angew. Chem. Int. Ed.* **2023**, *62*, e202301253.
- [94] M. P. Mercer, M. Nagarathinam, E. M. Gavilán-Arriazu, A. Binjraja, S. Panda, H. Au, M. Crespo-Ribadeneyra, M.-M. Titirici, E. P. M. Leiva, H. E. Hoster, *J. Mater. Chem. A* **2023**, *11*, 6543–6555.
- [95] J. L. Hutter, J. Bechhoefer, *Rev. Sci. Instrum.* **1993**, *64*, 1868–1873.
- [96] S. Frittmann, V. Halka, C. Jaramillo, R. Schuster, *Rev. Sci. Instrum.* **2015**, *86*, 064102.
- [97] C. H. Wang, D. Y. Gui, Q. Xia, M. Avdeev, C. D. Ling, B. J. Kennedy, *Inorg. Chem.* **2020**, *59*, 14439–14446.
- [98] K. Palanisamy, S. Daboss, D. Schäfer, M. Rohnke, L. Derr, M. Lang, R. Schuster, C. Kranz; **2023**; Spray-coated Hard Carbon Composite Anodes for Sodium-Ion Insertion; Kadi4Mat POLiS; ID 350, DOI: 10.5281/zenodo.8344722.

Manuscript received: September 14, 2023  
Revised manuscript received: October 20, 2023  
Accepted manuscript online: October 24, 2023  
Version of record online: ■■, ■■



*K. Palanisamy, Dr. S. Daboss, D. Schäfer, Dr. M. Rohnke, L. Derr, Dr. M. Lang, Prof. Dr. R. Schuster, Prof. Dr. C. Kranz\**

1 – 14

## Spray-coated Hard Carbon Composite Anodes for Sodium-Ion Insertion



**Spray coating:** The study presents a cost-effective, spray-coating process for HC composite electrodes on copper current collectors using different binder content and particle

sizes with controlled film thicknesses and mass loading. The spray-coated anodes revealed excellent performance.